ACS APPLIED MATERIALS & INTERFACES

Research Article

www.acsami.org

Chemical Strategies for Enhancing Activity and Charge Transfer in Ultrathin Pt Nanowires Immobilized onto Nanotube Supports for the Oxygen Reduction Reaction

Luyao Li,[†] Haiqing Liu,[†] Lei Wang,[†] Shiyu Yue,[†] Xiao Tong,[‡] Tatiana Zaliznyak,[§] Gordon T. Taylor,[§] and Stanislaus S. Wong*[,†,∥]

[†]Department of Chemistry, State University of New York at Stony Brook, Stony Brook, New York 11794-3400, United States

[‡]Center for Functional Nanomaterials, Building 735, Brookhaven National Laboratory, Upton, New York 11973, United States

[§]School of Marine and Atmospheric Sciences, State University of New York at Stony Brook, Stony Brook, New York 11794-5000, United States

[∥]Condensed Matter Physics and Materials Science Division, Brookhaven National Laboratory, Building 480, Upton, New York 11973, United States

Supporting Information

ABSTRACT: Multiwalled carbon nanotubes (MWNTs) represent a promising support medium for electrocatalysts, especially Pt nanoparticles (NPs). The advantages of using MWNTs include their large surface area, high conductivity, as well as long-term stability. Surface functionalization of MWNTs with various terminal groups, such as −COOH, −SH, and $-NH_2$, allows for rational electronic tuning of catalyst−support interactions. However, several issues still need to be addressed for such systems. First, over the course of an electrochemical run, catalyst durability can decrease, due in part to metal NP dissolution, a process facilitated by the inherently high surface defect concentration within the support. Second, the covalent functionalization treatment of MWNTs adopted by most groups tends to lead to a loss of structural integrity of the nanotubes (NTs). To mitigate for all of these issues, we have utilized two different attachment approaches (i.e., covalent versus noncovalent) to functionalize the outer walls of pristine MWNTs and compared the catalytic performance of as-deposited ultrathin (<2 nm) 1D Pt nanowires with that of conventional Pt NPs toward the oxygen reduction reaction (ORR). Our results demonstrated that the electrochemical activity of Pt nanostructures immobilized onto functionalized carbon nanotube (CNT) supports could be dramatically improved by using ultrathin Pt nanowires (instead of NPs) with noncovalently (as opposed to covalently) functionalized CNT supports. Spectroscopic evidence corroborated the definitive presence of charge transfer between the metal catalysts and the underlying NT support, whose direction and magnitude are a direct function of (i) the terminal chemistry as well as (ii) the attachment methodology, both of which simultaneously impact upon the observed electrocatalytic performance. Specifically, the use of a noncovalent $\pi-\pi$ stacking method coupled with a −COOH terminal moiety yielded the highest performance results, reported to date, for any similar system consisting of Pt (commercial NPs or otherwise) deposited onto carbon-based supports, a finding of broader interest toward the fabrication of high-performing electrocatalysts in general.

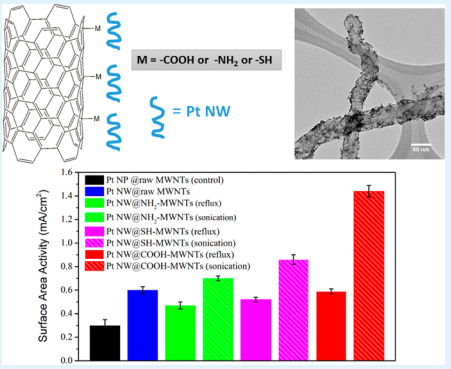

KEYWORDS: *Pt ultrathin nanowires, functionalized carbon nanotubes, noncovalent attachment, charge transfer, oxygen reduction reaction*

1. INTRODUCTION

A growing demand for efficient, low-cost renewable energy has sparked great interest in the research and development of fuel cell technology as a replacement for combustion-based energy sources.[1] A fuel cell is an electrochemical device that converts chemical energy via an oxidation process (at the anode) and a corresponding reduction (at the cathode) of a fuel into electrical energy. A prominent example of a functional fuel cell configuration is the proton exchange membrane fuel cell (PEMFC).[2−4] In PEMFCs, the oxygen reduction reaction (ORR), localized at the cathode, requires higher overpotentials in order to initiate the reaction as compared with the hydrogen oxidation reaction (HOR) occurring at the anode, and therefore denotes the rate limiting "step".[5] In other words, the process required to initiate ORR is especially energy intensive. Not surprisingly, the development of new and more effective electrocatalysts at the cathode has received significant research and developmental attention.[6]

Received: June 28, 2016
Accepted: November 23, 2016
Published: December 12, 2016

DOI: 10.1021/acsami.6b07870
ACS Appl. Mater. Interfaces 2016, 8, 34280−34294

State-of-the-art cathodic electrocatalysts primarily consist of nanostructured precious metals (e.g., Pt) and associated metal alloys supported onto commercial carbon supports, due to their high catalytic activity and reasonable durability in a highly acidic, high-oxygen concentration environment. Specifically, a lot of work has centered on anisotropic one-dimensional structures, such as nanowires (NWs) and nanotubes (NTs), because crystalline 1D nanostructures possess higher aspect ratios, fewer lattice boundaries, longer segments of smooth crystal planes, and a lower number of surface defect sites than their nanoparticulate (NP) analogues, all of which denote advantageous attributes for fuel cell catalysts.[7−10]

In particular, in our lab, we have expended a good deal of effort in developing ultrathin Pt-based nanowires (average diameters less than 5 nm) as viable structural motifs to not only maximize the surface area-to-volume ratio but also decrease the amount of catalytically inaccessible material within the interior of the wire. The inherent structural traits of ultrathin nanowires can induce superior activity in these systems as compared with both larger Pt nanotubes, as well as Pt nanoparticles.[11] As one key salient example relevant to the current paper, we demonstrated that our ultrathin, acid-treated, unsupported nanowires could achieve a surface area activity value of as high as 1.45 mA/cm^2, which was nearly 4 and 7 times greater than that of analogous, unsupported 200 nm-diameter Pt NTs and of supported commercial Pt NPs (∼3 nm in average diameter, immobilized onto a Vulcan XC-72 substrate with a Pt loading of 20% by mass), respectively.

While these advances in catalyst synthesis are important and necessary, the fundamental challenge remains as to how to maintain or improve catalyst activity and durability, while simultaneously reducing or eliminating Pt loading. One intriguing approach is to develop an "optimized" support material onto which these Pt NPs, NWs, and NTs are immobilized. Specifically, the conventional commercial supporting material itself, such as Vulcan carbon, can be prone to undergo damage and destruction in acidic media. In other words, even though carbon black (CB) can potentially assist in minimizing catalyst aggregation and dissolution, it unfortunately is also susceptible to undergoing electrochemical oxidation to surface oxides and ultimately, to CO_2. Indeed, catalyst failure can often be attributed to the corrosion of carbon substrates. Specifically, the structural and chemical integrity of traditional carbon-supported catalysts can be affected by changes in temperature, pH, and potential in addition to the water content and purity of the immobilized catalyst itself.[12]

The idea to mitigate for all of these issues would be to rationally design supports for which one can induce favorable catalyst−support interactions. Carbon nanotubes (CNTs) represent a model support medium for ORR catalysts because of a number of desirable attributes, including but not limited to their high surface area, reasonable electronic conductivity, as well as their relatively high stability and corrosion resistance when exposed to an acidic environment.[13−16] Multiwalled carbon nanotubes (MWNTs) are typically used by comparison with either their single-walled or double-walled CNT counterparts, since MWNTs are known to be durable and conductive as well as structurally robust, and can be more uniformly dispersed within a functioning reaction environment.[17]

As opposed to raw unprocessed CNTs, surface functionalized CNTs are even more appealing as catalyst supports due to their potential for "anchoring" and favorably influencing the subsequent activity and robustness of immobilized catalyst particles, such as Pt NPs.[12] For instance, theoretical DFT calculations[18] have predicted that the presence of SH groups on CNTs can not only restrict particle migration but also enhance the oxidative resistance of Pt clusters attached onto these derivatized CNTs. Specifically, by inhibiting Pt−O and Pt−OH formation, the greater observed stability of this architecture likely emanates from (i) an increased interaction between Pt and SH−CNTs, as well as from (ii) a depressed *d*-band center of the Pt NPs.

Hence, surface functionalization of either the support or the catalyst particle itself should hopefully help to achieve (a) a more uniform dispersion of metallic catalysts, as well as (b) protection from both dissolution and/or degradation, thereby implying higher durability as compared with their pristine counterparts.[19,20] An additional benefit that we seek to fully explore herein would be the presence of chemically induced electrocatalytic enhancement, which could be ascribed to favorable electronic interactions between the associated catalyst and the underlying substrate.

Experimentally, the nature of the surface functionalization yields a number of interesting results. As an example, Pt particles have previously been immobilized onto CNTs using an intervening triphenylphosphine (PPh_3) linker, because the PPh_3 moiety can assist in solubilizing Pt, prevent its aggregation, and furthermore, help in creating a uniform distribution of NPs on the underlying CNT surface, which collectively increase their intrinsic tolerance to impurity carbonaceous species.[21] Other relevant examples include the use of polymers,[22] such as ionic-liquid polymers (PIL),[23,24] as well as small organic molecules, such as 4-nitrophenyl groups,[25] sodium dodecyl sulfate,[26,27] and phthalocyanines,[28] to facilitate the immobilization of Pt NPs onto the CNT surface.

Using X-ray photoelectron spectroscopy (XPS), Guo et al. found that PtRu catalysts anchored onto carbon nanotubes, functionalized by both thiol groups (SH) and carboxylic acid groups (COOH), show varying affinities in terms of binding potentially poisonous CO species. Specifically, based upon the Pt $4f_{7/2}$ peak shifting to a higher binding energy for the −SH functionalized CNTs, it was suggested that back-donation from the Pt to the CO was lessened, because Pt interacts strongly with −SH. Such a scenario ultimately resulted in a favorably weakened binding of Pt to CO as compared with the corresponding COOH-functionalized CNTs. Guo's work also provided important insight into the direction of charge transfer within the functionalized CNT-based heterostructures. In effect, the S 2p shift to lower energy within SH−CNT relative to that of Pt−SH−CNT itself implied charge movement from the catalytic Pt NPs to the attached SH−CNT support.

These XPS data collectively illustrate that surface terminating moieties can not only facilitate the dispersion of the NPs onto the underlying support but also can affect the catalyst's inherent electronic character, all of which have a direct impact upon catalysis.[29] Hence, the focus of this paper is on systematically understanding the important and perhaps less well-understood "intermixing" of the electronic structures of the immobilized catalysts with that of the underlying catalytic supports. We intend to probe these relatively poorly understood interactions as a function not only of the precise terminal chemistry of the CNT supports themselves but also of the exact means used to couple our Pt catalysts with the underlying CNT surfaces.

Most of the prior literature has focused on forming covalent linkages between the MWNTs and their terminal end groups.

DOI: 10.1021/acsami.6b07870
ACS Appl. Mater. Interfaces 2016, 8, 34280−34294

Scheme 1. Synthesis Process of COOH, NH_2, and SH-MWNTs, Respectively, Generated Using a Covalent "Reflux-Mediated" Method

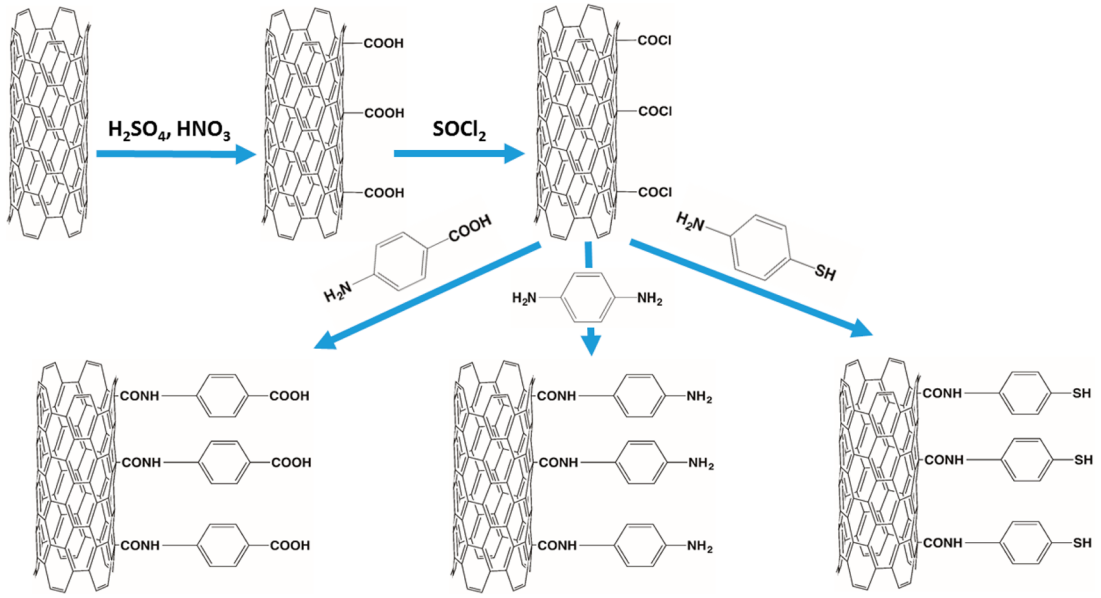

Specifically, MWNTs have been initially oxidized to yield oxygenated carboxylic acid groups on their outer surface (i.e., COOH−MWNTs) and then further modified with an array of additional functional groups, such as but not limited to hydroxide (−OH), thiol (−SH), and amine ($-NH_2$) moieties.[30,31] Nonetheless, studies have demonstrated that such harsh surface modifications can give rise to two main disadvantages. First, the initial acid treatment may inevitably engender an increase in the number and percentage of surface defects on the MWNTs, which in turn can cause the loss of both conductivity and structural integrity of the nanotubes, thereby resulting in a loss of activity as well as of long-term stability.[32] Moreover, dangling bonds formed during the covalent functionalization process can easily be oxidized and thereby induce a greater degree of surface corrosion under standard electrochemical conditions.[33] Second, the carboxyl groups tend to localize onto existing defect sites, which may affect the resulting dispersion of deposited Pt nanostructures.

Herein, we have utilized two distinctive methods (i.e., a *covalent*, reflux-mediated approach versus a *noncovalent*, sonication-based technique) of coupling MWNTs with the various types of ligands that contains common terminal functional groups, including carboxylic acids, amines, and thiols. We found that these *noncovalently* generated supports display superior performance toward ORR as compared with their *covalently formed*, reflux-based CNT counterparts. We have subsequently probed the electronic structures of the as-formed catalyst−support combinations, through optical characterization techniques including XPS and Raman spectroscopy. As a model system, we have deposited our as-prepared ultrathin (average diameter ∼2 nm) Pt nanowires onto these variously functionalized MWNTs to investigate the impact of modifying not only (a) the terminal ligand moiety but also (b) the attachment approach. That is, we view the purposeful alteration of the substrate's electronic structure as an attractive and perhaps less studied variable with which to enhance electrocatalytic performance.

Moreover, as an additional and key element of novelty within our work, we highlight that prior studies have usually analyzed the deposition of Pt NPs onto various types of substrates (i.e., our control experiments herein). By contrast, we have focused our efforts on our high-performing, as-prepared ultrathin Pt NWs. Hence, for the first time, we have investigated hitherto unknown NW catalyst-functionalized MWNT support interactions in ORR. Our results indicate that electron transfer processes do in fact occur in these systems, due to the presence of the various terminal functionalities. Most interestingly, not only the direction of the observed charge transfer but also the observed ORR performance appears to depend to a large degree on the precise attachment (i.e., covalent vs noncovalent) methodology used to connect the NW catalyst with the underlying catalyst support.

In terms of activity benchmarks, the specific activities of Pt NPs supported on MWNTs usually vary in a range from 0.3 to 0.6 mA/cm^2, depending upon the specific surface modifications of the supports, which are respectively characterized by pendant $-NH_2$, −COOH, −OH, and −SH moieties.[30,31,34,35] Herein, our best result was noted with Pt NWs dispersed onto COOH-functionalized MWNTs with a physical sonication method. In effect, the measured activity (i.e., 1.54 mA/cm^2) on these derivatized supports was more than (i) 2-fold greater as compared with similarly dispersed Pt NWs on raw MWNTs and more than (ii) 5-fold higher than what is normally associated with conventional Pt NPs supported onto raw MWNTs. Moreover, to the best of our knowledge, our data have surpassed any previously reported results on comparable systems composed of nanoscale Pt metal catalysts coupled with carbonaceous supports. We believe that this reproducible enhancement originates from a positively synergistic and favorable interaction between morphological and chemical effects. Moreover, our data may also yield promise for the development of 1D-1D heterostructures as architecturally viable electrochemical motifs.

2. EXPERIMENTAL SECTION

2.1. Synthesis of Various Functionalized MWNTs. *2.1.1. Chlorinated MWNTs as an Intermediate Using a Covalent "Reflux" Method.* Initially, 100 mg of pristine MWNTs (SSE, outer

DOI: 10.1021/acsami.6b07870
ACS Appl. Mater. Interfaces 2016, 8, 34280−34294

diameter of 10−30 nm) was mixed with 25 mL of H_2SO_4 (Sigma, 95−98%)/HNO_3 (Fisher, 70%) (3/1, volume ratio) and sonicated until the MWNTs were completely dissolved in acid. After refluxing at 80 °C for 4 h with gentle stirring at 400 rpm, the mixture was diluted by 500 mL of distilled, deionized (DI) water and then vacuum-filtered through a 200 nm polycarbonate membrane. The solid was subsequently dried at 70 °C for 24 h.[36] As shown in Scheme 1, MWNTs with surface carboxyl groups can indeed be obtained after acid treatment. However, in order to normalize the surface chemical protocols used and thereby allow for a meaningful comparison among all of our samples, we simply used this carboxylated product as a precursor to the production of a chlorinated intermediate MWNT species for the subsequent creation of amine, thiol, and carboxylated MWNTs, respectively.

Therefore, to generate the chlorinated MWNTs, 20 mg of as-prepared solid product was mixed with 10 mL of thionyl chloride ($SOCl_2$, Aldrich, 99.5%) and refluxed at 70 °C for 24 h with stirring at 400 rpm. The mixture was then added dropwise into methanol; a black precipitate solid could be isolated from the solvent upon centrifugation at 3000 rpm for 10 min. This product was later washed with methanol for several times and ultimately dried at 70 °C for 12 h.[37]

2.1.2. Thiol, Amine, and Carboxyl-Terminated MWNTs Using a Covalent "Reflux" Method. In obtain the desired *thiolated* carbon nanotubes (SH-MWNTs), 10 mg of as-prepared chlorinated-MWNTs and 4-aminothiophenol ($NH_2-C_6H_4-SH$, Acros Organics, 96%)[38] were dissolved in 20 mL of dehydrated toluene (Acros, 99+%) at 70 °C for 24 h. Analogous *amine-terminated* MWNTs were prepared using a similar method by mixing 10 mg chlorinated MWNTs with *p*-phenylenediamine ($NH_2C_6H_4NH_2$, Sigma) in 20 mL of dehydrated toluene (Acros, 99+%) at 70 °C for 24 h. Lastly, *carboxylic acid-derivatized* carbon nanotubes (COOH−MWNTs) were produced by mixing 10 mg of chlorinated MWNTs with 4-aminobenzoic acid ($NH_2-C_6H_4-COOH$, Aldrich, 99%) in 20 mL of dehydrated toluene (Acros Fisher, 99+%) at 70 °C for 24 h.

2.1.3. Carboxyl-Terminated MWNTs Using a Noncovalent "Sonication" Method. Raw MWNT powder and *p*-aminobenzonic acid ($NH_2C_6H_4COOH$, Aldrich, 99%) were dissolved within a mixture of ethanol (Alfa Aesar, 90%) and toluene (Acros, 99+%) characterized by a volume ratio of 1:2. The whole mixture was then sonicated (Branson 1210 Ultrasonic Cleaner, run at 40 kHz) for 4 h, and the resulting precipitate was separated from the mixture by a centrifugation process, run at 3000 rpm for 10 min. The product was subsequently washed with ethanol, and centrifuged again at 3000 rpm for three separate times. The *carboxylic acid-derivatized* product was ultimately oven-dried at 70 °C for 12 h.

2.1.4. Synthesis of Amine and Thiol-Terminated MWNTs: Noncovalent "Sonication" Method. *Thiol-terminated* MWNTs were synthesized by initially mixing raw MWNTs with 4-aminothiophenol ($NH_2C_6H_4SH$, Acros Organics, 96%) dissolved in 20 mL of dehydrated toluene (Acros, 99+%), followed by physical sonication under room temperature conditions for 3 h. *Amine-derivatized* MWNTs were created by an identical procedure except with the use of *p*-phenylenediamine ($NH_2C_6H_4NH_2$, Sigma) as the precursor reagent. In both cases, the final products were washed with ethanol and later dried at 70 °C for 12 h.

2.2. Synthesis of Ultrathin Pt Nanowires. Ultrathin Pt nanowires were synthesized using a modification of the phase-transfer method previously reported by Teng et al.[39] First, 29 mg (0.05 mmol) of hexachloroplatinic acid hydrate ($H_2PtCl_6{\cdot}6\,H_2O$, Alfa Aesar, 99.9%) were combined with 400 mg of ODA (octadecylamine, Acros Organics, 90%), and 60 mg of DTAB (*n*-dodecyltrimethylammonium bromide, TCI) in a 100 mL round-bottom flask and ultimately dissolved in 7 mL of toluene (Acros Organics, 99+%) under vigorous magnetic stirring at 400 rpm. The whole mixture was then sonicated for 20 min and degassed under argon for three times using a standard Schlenk-line procedure. The reducing agent, consisting of 13 mg sodium borohydride ($NaBH_4$, Alfa Aesar, 98+% powder), was first dissolved in 2 mL of DI water and then added into the mixture dropwise while stirring. The synthesis reaction was subsequently run under an Ar atmosphere at room temperature for 1 h.

Aliquots of 2 mL of DI water and 2 mL of chloroform were subsequently added to separate the aqueous phase and the organic phase. After 5 min of sonication, followed by 10 min of centrifugation at 9000 rpm, a black organic phase, containing Pt nanowires, was isolated and then washed with ethanol for multiple times. A black solid consisting of Pt nanowires was ultimately obtained after centrifugation.

2.3. Deposition of Ultrathin Pt Nanowires onto Variously Functionalized MWNTs. Ultrathin Pt nanowires were deposited onto various supports by a simple method, previously reported by our group. Specifically, as-prepared Pt nanowires were redispersed in 6 mL chloroform. In independent experiments, an equal mass of 6 mg of the different carbon nanotube supports, including raw MWNTs as controls (Figure S1), was separately added, followed by 30 min of bath sonication and 40 min of centrifugation at 9000 rpm. The resulting nanowire-support composites were stored in hexane for 12 h, prior to electrochemical analysis.

2.4. Deposition of Pt Nanoparticles onto Raw MWNTs−Control Experiment. Raw MWNTs onto which a sample of Pt nanoparticles had been supported were synthesized as a control sample (Figure S1). Specifically, 29 mg of hexachloroplatinic acid hydrate ($H_2PtCl_6{\cdot}6\,H_2O$, Alfa Aesar, 99.9%) and 6 mg of raw MWNTs were added together into 50 mL of deionized H_2O. Under vigorous stirring, 13 mg of $NaBH_4$ was included in the mixture as a reducing agent, and the reaction proceeded for 15 min under vigorous stirring. After that step, the resulting product was subsequently vacuum filtered through a 200 nm diameter pore-size polycarbonate membrane, washed with deionized water, and ultimately vacuum-dried at 90 °C for 3 h.

2.5. Structural Characterization. *2.5.1. TEM Imaging.* The morphology of electrocatalytic samples was characterized using a JEOL 1400 transmission electron microscope, equipped with a 2048 × 2048 Gatan CCD camera and operated at an accelerating voltage of 120 kV. Samples were prepared by simply dissolving powder samples in ethanol followed by drop casting onto a copper grid.

2.5.2. Thermogravimetric Analysis. The Pt loading of each sample was quantified using a TGA Q500 instrument (TA Instruments). Specifically, powders of the different samples were individually placed onto a Pt boat. Isotherms were acquired by controllably increasing the temperature from room temperature to 1000 °C at a ramp rate of 10 °C/min in extra-dry air (i.e., compressed air from Praxair, 1 ppm of H_2O by volume), pumped into the system at a rate of 40 mL/min. Weight loss profiles were plotted using the Origin 8.0 software. The actual Pt loading values were determined on the basis of at least two separate runs.

2.5.3. Raman Spectroscopy. For the variously functionalized MWNTs, Raman spectroscopy has been utilized to probe modifications in the characteristic CNT signature as a function of not only the various surface ligands but also the different functionalization methods, so as to gauge what effects rational chemical modification of the CNT surface might have on the inherent structure of carbon nanotubes. We postulate that rational alterations in chemistry can be used to "tune" the ORR activity of MWNTs.

The integrity of both pristine and variously functionalized MWNTs was examined by a Renishaw inVia high resolution confocal Raman microscope outfitted with a Leica DM2500 upright microscope and fitted with an automated *xyz*-motorized stage. The data were collected using a 514.5 nm (2.41 eV) in line laser, and the wavelength and intensity calibrations were completed by using an internal silicon standard, based upon a reference peak at 520 cm^{-1}. Raman samples were prepared by dropping aliquots of an ethanolic dispersion of the MWNTs (both with and without Pt deposition) onto Si substrates (measuring 1 cm × 1 cm) followed by drying in air at room temperature.

Spectra from the samples were collected using an 1800 line/mm grating, resulting in a spectral resolution of ∼0.5 cm^{-1}, with a 30 s integration time per spectrum using a CCD array. As-obtained spectra were subsequently processed and analyzed using the WiRE 4.1 software. Baselines were subtracted from all of the spectra, and the integrated spectral areas were normalized to an area of 1. Resulting peaks were fitted with Lorentzian curves in order to determine the

DOI: 10.1021/acsami.6b07870
ACS Appl. Mater. Interfaces 2016, 8, 34280−34294

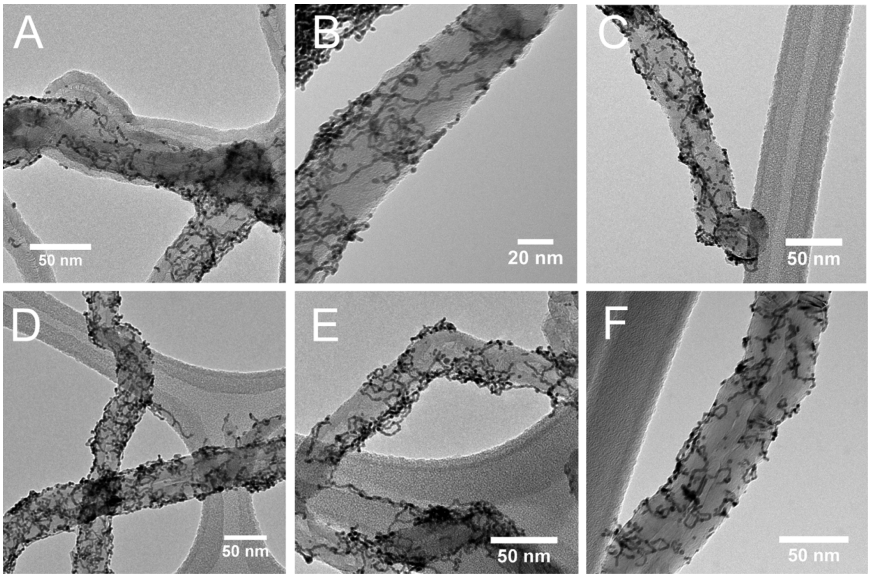

Figure 1. TEM images of Pt NWs supported onto variously functionalized MWNTs using the covalent "reflux-mediated" method (A–C) and the noncovalent "physical sonication-based" method (D–F), respectively. The functional groups introduced onto the surfaces of the MWNTs include carboxylic acid (A and D), amine (B and E), and thiol (C and F) species, respectively.

peak position, integrated areas (intensity), and peak widths, respectively.

2.5.4. XPS Measurements. XPS was utilized to confirm the successful surface conjugation and attachment chemistry of our MWNTs. Moreover, XPS was used as a technique to gauge the degree of electronic interaction between the immobilized Pt nanowires and the different underlying functional groups on the MWNT surface.

XPS samples were prepared by dispersing powder samples (both with and without Pt deposition) in a small amount of ethanol and dripping aliquots of that solution onto a Si wafer (measuring 1 cm × 1 cm) followed by drying in air. Samples were then placed into the vacuum chamber of a home-built XPS surface analysis system equipped with a model SPECS Phoibos 100 electron energy analyzer for electron detection. The chamber was evacuated to a base pressure of about 2×10^{-10} Torr. XPS spectra were first collected using an Mg Kα X-ray source ($h\upsilon$ = 1253.6 eV) (model XR 50) under operating conditions of 10 kV and 30 mA. The angle between the analyzer and the X-ray source is 45°, and photoelectrons were acquired along the sample's surface normal vector.

In the data analysis, the C 1s peak was set at a position of 284.5 eV,[40] to subsequently calibrate the relative positions of the Pt 4f peak, the N 1s peak, and the S 2p peak, respectively. The Shirley background was then subtracted away, and curve fitting was performed using the XPS PEAK software. Accurate positions for the Pt 4f peak, the N 1s peak, and the S 2p peak were automatically determined by the software after curve fitting. Final processed data were plotted using the Origin 8.0 software.

2.6. Electrochemical Measurements. *2.6.1. Activating the Surfaces of As-Prepared Electrocatalysts.* Prior to electrochemical characterization, both as-prepared as well as functionalized MWNTs incorporating supported Pt nanowires were rendered into catalyst inks by dispersing the dry powders into ethanol so as to create an approximately 2 mg/mL solution, as a general guideline for all samples processed. Before application of the nanowire ink, a glassy carbon rotating disk electrode (GC-RDE, Pine Instruments, 5 mm inner diameter, surface area of 0.196 cm^2) was polished until a pristine finish was obtained.

Then, two 5 μL drops of the dispersed catalyst ink were drop-cast onto the electrode, while the electrode was maintained at a rotating speed of ~800 rpm in order to ensure uniformity of the thickness of the as-deposited catalyst layer; these droplets were essentially allowed to air-dry. Once dried, the electrode was sealed with one 5 μL drop of an ethanolic 0.025% Nafion solution prepared from a 5% stock solution (Aldrich, Nafion 117 solution).

Electrochemical measurements were obtained in a 0.1 M perchloric acid (Fisher Scientific, Optima grade) solution generated using high-purity type 1 water, possessing a high resistivity of 18.2 MΩ·cm. An Ag/AgCl (3 M Cl^-) combination isolated in a double junction chamber (Cypress) and a platinum foil served as the reference electrode and the counter electrode, respectively. All of the potentials reported in this paper have been recorded with respect to the reversible hydrogen electrode (RHE), unless otherwise mentioned.

The ODA capping agent and other organic impurities on as-prepared ultrathin NWs were removed by a selective CO adsorption process, that we have successfully utilized in the past.[41] Briefly, the MWNT-supported nanowires were deposited onto a glassy carbon electrode, and the potential was cycled in deoxygenated 0.1 M $HClO_4$ within a potential range of 0 to 1.3 V (vs RHE) at a rate of 100 mV/s, until a stable profile was obtained. For all samples analyzed, each cycling process attained a total of 50 cycles. Thereafter, the electrode was immersed in a CO-saturated electrolyte for a period of 30 to 45 min so as to selectively displace residual organic impurities from the surfaces of the NWs. The electrode was then washed in ultrapure water and transferred to a freshly deoxygenated electrolyte, wherein a CO stripping cyclic voltammogram (CV) was run by cycling the potential within the range of 0 to 1.15 V (vs RHE). The combination of running CO adsorption and stripping processes was repeated for an additional two more times or until the CO stripping profile itself was deemed to be reproducible.

2.6.2. Electrochemical Characterization. The measurements of the ORR performance for the various catalyst samples were carried out by employing a thin-layer rotating disk electrode method. Initially, CVs were obtained in a deoxygenated (i.e., carried out by purging Ar gas through the electrolyte for a minimum of 15 min) electrolyte solution at a scan rate of 20 mV/s, so as to establish the basis for calculating the associated electrochemical surface area (ECSA). Then, the ORR activity of the various catalyst samples was measured by obtaining polarization curves in oxygen-saturated electrolytes at 20 °C with the electrode rotated at a rate of 1600 rpm and the potential scanned at a rate of 10 mV/s. The kinetic current density was evaluated using the Koutecky–Levich relationship, and these data were subsequently normalized to the ECSA of the catalyst loaded onto the GCE in order to determine the surface area-normalized kinetic current (J_k) densities. To ensure the reproducibility of results, each experiment was performed for up to three times. Moreover, at least one of these

DOI: 10.1021/acsami.6b07870
ACS Appl. Mater. Interfaces 2016, 8, 34280–34294

runs was carried out by preparing a different electrode on a different day than that of the original experiment, in order to certify the validity and reliability of the overall data set. Reported error bars originate from the standard deviations of the various measurements.

Durability testing was conducted on a sample of Pt NW@COOH-MWNT electrocatalysts under half-cell conditions in perchloric acid by utilizing a durability test protocol standard, previously described by the U.S. Department of Energy for simulating a catalyst lifetime under realistic membrane electrode assembly operating conditions. Specifically, the potential was cycled from 0.6 to 1.0 V (vs RHE) in an acidic 0.1 M $HClO_4$ medium that had been left open to the atmosphere. Data on ECSA and the corresponding electrochemical surface area activity were obtained after successive 5000 cycles.

3. RESULTS AND DISCUSSION

3.1. Structural Characterization. *3.1.1. Electron Microscopy and TGA.* TEM images of Pt nanowires deposited on the various supports synthesized by both the "covalent reflux-mediated" method (Figure 1A−1C) and the "noncovalent sonication-induced" method (Figure 1D−1F) indicate that the average diameters of these ultrathin Pt NWs are all ∼2 nm, as expected and regardless of the support used. These data also confirm the 1D nature and the structural integrity of the ultrathin Pt catalysts analyzed.

The TEM images of Pt NP@raw MWNTs and of Pt NW@raw MWNTs are included as components of Figure S1 (Supporting Information section), as they provide visual evidence for a reasonable dispersion of nanowires on the underlying nanotubes. Our current results are consistent with analogous experiments previously reported in the literature, and serve as a check on the validity of our subsequent data interpretation.[42,43] Hence, our focus herein will be on analyzing the Pt NWs supported onto variously functionalized MWNTs.

The actual Pt loadings by weight were determined by means of thermogravimetric analysis (Figure S2). All profiles indicate a typical "three-step" weight loss process, regardless of either the functionalization method used or the terminal surface moieties involved. For covalent "reflux"-synthesized supports, surfactants and water were initially oxidized and evaporated off in the first step (i.e., below 150 °C). Functional groups were subsequently annealed away and presumably removed during the temperature interval from 150 to 400 °C. The last step involved the combustion of the MWNTs themselves from 400 to 600 °C. The weight of the residue remained at a relatively stable level thereafter, and hence, it was plausibly ascribed to the presence of elemental Pt (and not to Pt oxides which would have already decomposed by that temperature).[44,45] Hence, the value for the exact loading of Pt NWs was taken as the "plateau" observed on the curve beyond 600 °C.

Based on this analysis, the final weight percentage values we found for Pt are 36.0 ± 1.4% for carboxyl-terminated MWNTs, 61.9 ± 2.9% for amine-terminated MWNTs, and 63.4 ± 2.3% for thiol-terminated nanotubes, respectively. For noncovalent, "sonication"-based substrates, the corresponding amounts of Pt we measured were 23.7 ± 1.0%, 33.1 ± 1.5%, and 42.8 ± 1.8% for carboxyl, amine, and thiol-terminated MWNTs, respectively. Although the amount of Pt nanowires varies to some degree for each sample, a prior study demonstrated that ORR activity is independent of Pt loading in the range of 20% to 60% (wt %).[46] Hence, by analogy, with our work, it is expected that the relatively small range and variation in terms of the different catalyst quantities immobilized on each of the variously functionalized MWNT surfaces involved herein will not necessarily affect their respective ORR performances, thereby rendering activity comparisons among our samples to be legitimate and interpretable.

Furthermore, we have conducted experiments with a series of variously processed Pt NW@raw MWNT nanocomposites to examine the impact of varying Pt NW loadings. As shown in Figure S3, changes in the Pt loadings appear to correlate with corresponding alterations in the magnitudes of the intensities of the features within the CV curves, a finding reflecting differences in the absolute capacitance values of the different samples in question. However, the polarization curves of all three Pt NW@raw MWNT samples, containing various Pt loadings ranging from 20% to 50%, are actually strikingly similar. As such, the calculated ORR specific activities are within systematic error, suggesting that for our ORR studies herein, the measured activity values are independent of the range of Pt loading used.

3.1.2. Spectroscopy. A representative deconvolution of the Raman spectra corresponding to both the pristine and functionalized MWNTs prepared using the covalent method (Figure 2A) and the noncovalent protocol (Figure 2B),

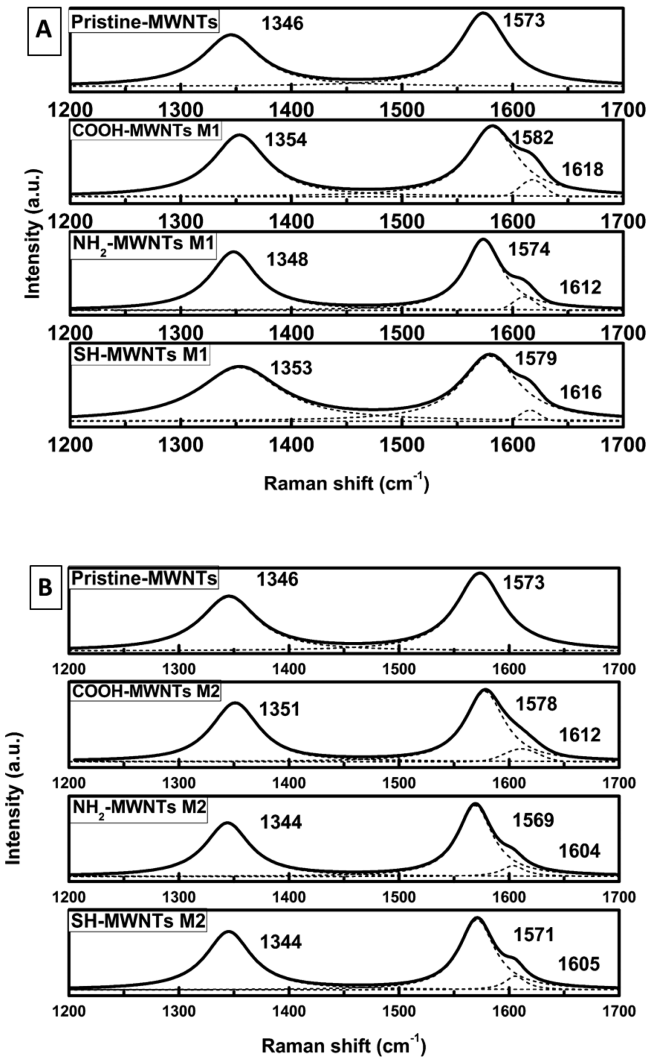

Figure 2. Raman D, G, and D′ band spectra measured at an excitation wavelength of 514 nm (2.41 eV) for pristine MWNTs, COOH-MWNTs, NH_2-MWNTs, as well as SH-MWNTs, prepared by (A) "covalent reflux-mediated" (M1 series) and (B) 'physical sonication-induced' (M2 series) methods, respectively.

DOI: 10.1021/acsami.6b07870
ACS Appl. Mater. Interfaces 2016, 8, 34280−34294

respectively, depicted three distinctive first-order Raman bands, namely the D band located at 1344 cm^{-1}, the G band localized at 1570−1580 cm^{-1} (i.e., the E_{2g} mode), as well as the D′ band placed at 1600−1610 cm^{-1}.[47] The D band arises from a sp^3-carbon disorder-induced feature, arising from the double resonance Raman scattering process associated with elastic phonon scattering close to the K and G points of the graphitic Brillouin zone. The G band originates from the "in-plane" tangential stretching vibrational mode, specifically, E_{2g}, of the carbon−carbon bonds within graphene sheets. The D′ band, which is also a double resonance feature induced by disorder and defects, stems from symmetry breaking, and appears as a shoulder of the G band at higher frequencies. All of the Raman spectra in Figure 2 have been normalized, such that qualitative trends associated with alterations in the intensities and positions of all bands can be properly visualized and interpreted. Detailed intensity profiles and peak positions of each band are summarized in Table 1. A few general observations and trends are noteworthy of mentioning.

Table 1. Raman Intensity Values and Intensity Ratios of the D-Band, the G-Band, and the D′-Band, Respectively, for Variously Functionalized MWNTs

sample name (with preparative method)	D-band intensity	G-band intensity	G-band position (cm^{-1})	I_D/I_G	D′-band intensity	$I_G/I_{D'}$
raw MWNTs	0.63	0.92	1573	0.685	N/A	N/A
COOH-MWNTs, reflux	0.82	0.96	1582	0.854	0.26	3.692
NH_2-MWNTs, reflux	0.80	0.97	1574	0.825	0.18	5.389
SH-MWNTs, reflux	0.71	0.89	1579	0.798	0.17	4.176
COOH-MWNTs, sonication	0.79	0.96	1578	0.823	0.15	6.400
NH_2-MWNTs, sonication	0.71	0.95	1569	0.747	0.13	7.308
SH-MWNTs, Sonication	0.77	0.94	1571	0.819	0.17	5.529

First, in terms of *peak intensity* (Table 1), as compared with raw MWNTs, the G band evinced little if any changes, while the D band and D′ band were enhanced dramatically with the covalently generated COOH-MWNTs, NH_2-MWNTs, and SH-MWNTs, respectively; the COOH-MWNT structures yielded the largest enhancement. It is worth noting that the NH_2-MWNTs and SH-MWNTs, functionalized through the noncovalent method (method 2), demonstrated noticeably less D and D′ band enhancements as compared with analogues prepared using the covalently inspired method (method 1).

The observed enhancements in the D and D′ band intensities can be potentially attributed to the presence of disordered carbon in the MWNTs because of functionalization processes, which can introduce defects including not only sp^3 hybridized carbon but also localized defects on the nanotube walls, including vacancies, heptagon-pentagon pairs, and heteroatoms.[48] The largest enhancements in the D and D′ band intensities associated with COOH-MWNTs can be possibly ascribed to higher coverage densities of the −COOH functional moieties, thereby resulting in a larger degree of disorder. The differences in the degree of enhancement of the D and D′ bands associated with the NH_2 and SH-functionalized MWNTs prepared using both covalent and noncovalent protocols, respectively, are not surprising, considering that the acid-functionalization step in the relatively more destructive reflux-mediated, covalent method tends to break apart the sp^2 C═C bond symmetry. By contrast, the noncovalent procedure utilizes pristine MWNTs, which likely interact with the various introduced functionalities through $\pi-\pi$ stacking and in so doing, retains and preserves the intrinsic sp^2-based symmetry of the MWNTs.

Second, in terms of *peak position* (Table 1), obvious up-shifts in all three bands (i.e., the D, D′, and G) are observed with the COOH, NH_2, and SH-functionalized MWNTs prepared using the reflux method. In effect, the upshift in the G band can be potentially attributed to electron transfer from the functionalized MWNTs to the attached NH_2 and SH functional moieties, thereby resulting in (i) a depletion in the electron occupation of the nanotube valence bands as the Fermi level is lowered, (ii) an effective shortening of the C−C bond distance, and therefore, (iii) a stiffening of the G mode.[49] As for the corresponding samples produced using the noncovalent method, we have observed the exact opposite behavior, as manifested by a G-band down-shift for NH_2 and SH-terminated samples, thereby implying an electron transfer from the terminal functionalized moieties to the underlying MWNTs. However, this trend does not necessarily apply to the COOH-functionalized sample. A detailed explanation in addition to a hypothesis for the observed electron transfer mechanism are presented in section 3.3.

Therefore, to provide additional insight into the chemical nature of our samples, XPS survey spectra were acquired. Figure 3 highlights XPS spectra of N 1s for NH_2-MWNTs and S 2p for SH-MWNTs, prepared by both covalent and noncovalent protocols. All four spectra showed well-defined peaks for these particular elements.

Specifically, for the NH_2-MWNT samples, two peaks, which can be ascribed to the N 1s signal, were identified for the covalently functionalized sample. In particular, a feature with a binding energy of 399.5 eV could be attributed to the presence of primary amines ($-CH_2-NH_2$), while a corresponding band at 401.9 eV could be assigned to the existence of amide groups (−CO−NH−).[50] By contrast, we noted that the noncovalently derivatized sample yielded only one amine peak, located at 399.4 eV, since no amide group was likely to have been generated, because the synthesis process itself did not involve formal bond formation. For both SH−MWNT samples tested, we observed two split doublet peaks (i.e., S $2p_{1/2}$ and S $2p_{3/2}$) which can be assigned to a R−S−H moiety, consistent with the expected presence of a terminal thiol group (-SH). Moreover, a small peak possessing a higher binding energy (i.e., 167.5 eV for covalently formed samples versus 168.7 eV for noncovalently functionalized MWNTs) could be ascribed to the presence of a S−O bond, likely formed in air.[51] However, since our primary goal has been to probe changes in the inherent electronic structure of Pt, we will be focusing on the behavior of the Pt 4f peaks.

Figure 4 denotes the positions of the Pt 4f peaks associated with Pt nanowires immobilized onto different supports. A down-shift in the binding energy position of the Pt $4f_{7/2}$ peak within these functionalized MWNT supports, especially as compared with Pt NW@ raw MWNT, can be observed in *some* of the samples (e.g., those with amine and thiol terminal functional groups). In general, the decrease in this binding energy value implies electron donation from the chemically

DOI: 10.1021/acsami.6b07870
ACS Appl. Mater. Interfaces 2016, 8, 34280−34294

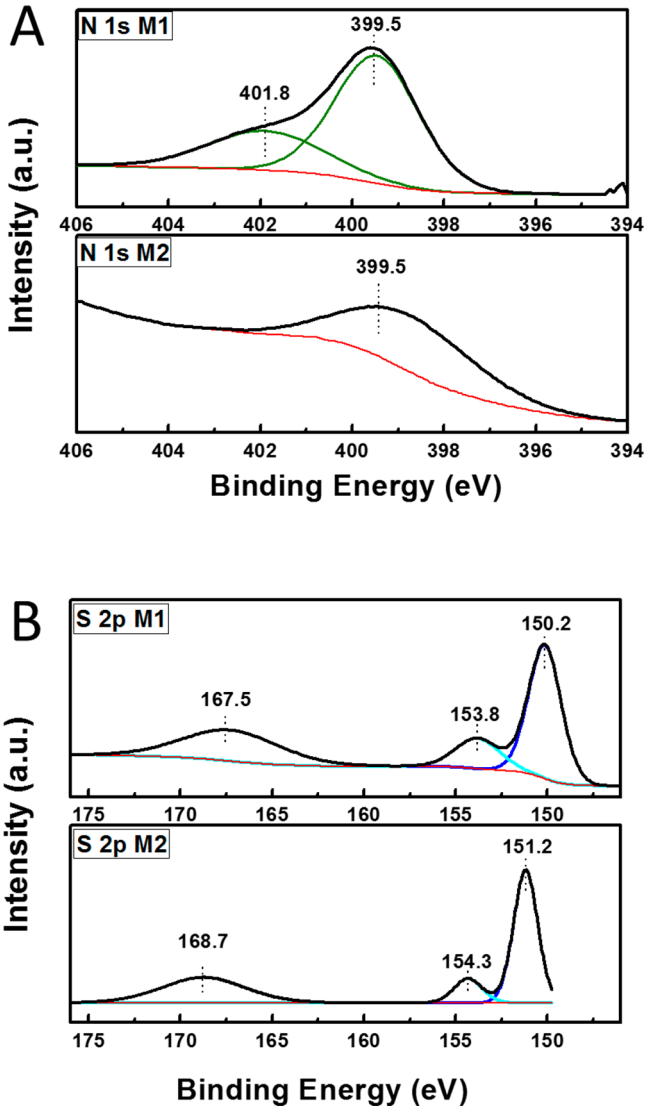

Figure 3. XPS spectra of (A) N 1s and (B) S 2p orbitals for corresponding NH_2-MWNT and SH-MWNT samples, prepared by both "reflux-mediated" methods (M1) and 'physical sonication-induced' (M2) techniques, respectively. Spectra were obtained by calibration based upon a binding energy value for C 1s of 284.5 eV.

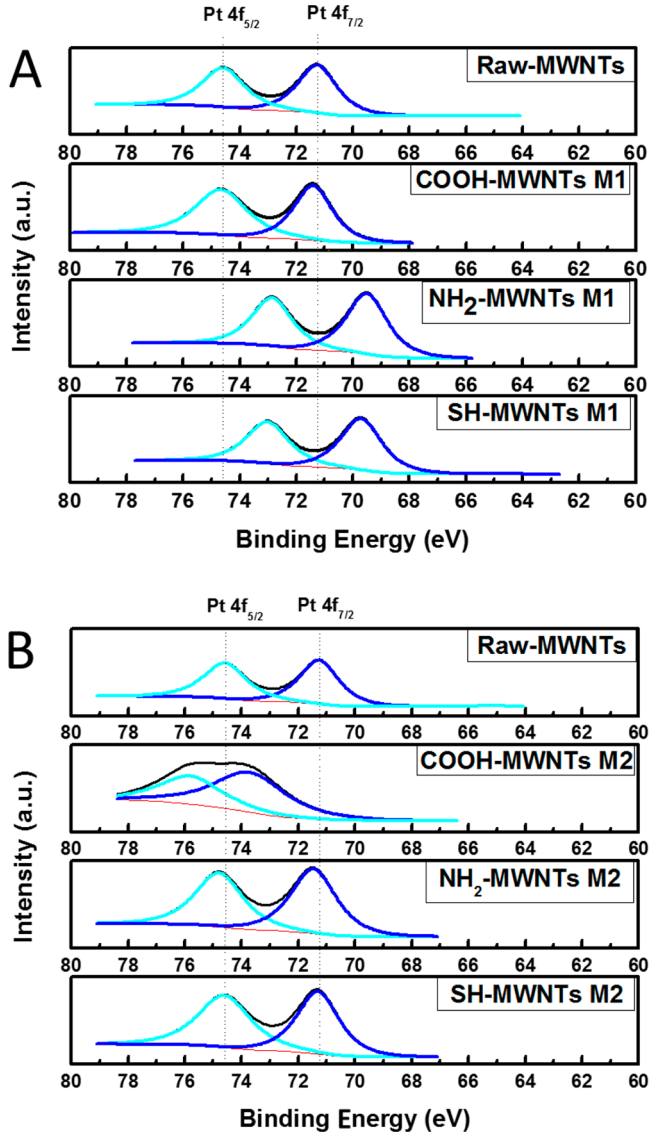

Figure 4. Pt 4f XPS spectra of pristine MWNTs and of functionalized MWNTs prepared by (A) the covalent, "reflux-mediated" (M1) method and (B) the noncovalent, "sonication-based" (M2) method. The XPS spectra were obtained by calibration, based upon a value for the C 1s binding energy of 284.5 eV.

functionalized carbon nanotube supports to the Pt catalysts and vice versa. Specifically, for the chemical "covalent reflux-mediated" method, COOH-MWNTs possess a similar Pt 4f binding energy (i.e., 71.3 eV) with that of raw MWNTs (i.e., 71.2 eV), whereas both NH_2-MWNTs (i.e., 69.5 eV) and SH-MWNTs (i.e., 69.7 eV) give rise to lower binding energies as compared with raw MWNTs, implying electron transfer from surface-modified MWNTs to the immobilized Pt.

By contrast, both NH_2-MWNT and SH-MWNT catalysts generated by the noncovalent method yielded a perceptible upshift (i.e., 0.3 eV) to 71.5 eV, while the COOH-MWNT catalysts evinced a more obvious upshift (i.e., 2.6 eV) to 73.8 eV as compared with raw MWNTs. Hence, the data for all 3 of these "noncovalent" samples imply charge transfer from Pt to the underlying MWNTs, indicative of the opposite trend to what was found for the "covalent", refluxed-mediated samples.

Analogous behavior has been previously observed in comparable systems wherein variations in the underlying substrates have yielded a corresponding alteration of the electronic structure of the as-deposited Pt electrocatalysts. Specifically, it has been reported that an upshift in the XPS peak is usually correlated with enhanced ORR activity. For instance, Awaludin et al. noted a positive shift (by 0.3 eV) of the position of the Pt 4f core level peaks within the $Pt/TaO_x/GC$ electrocatalyst, as compared with that of bulk Pt. This spectroscopic shift in peak position was accompanied by a greater than 8-fold increase in specific activity as compared with Pt/carbon.[52]

Similarly, Zhang et al. have reported that the positions of the Pt $4f_{7/2}$ and $4f_{5/2}$ peaks shifted from 71.3 to 71.5 eV, as well as from 74.5 to 74.7 eV, respectively, when analyzing Pt_3Ni nanoparticles supported onto carbon versus those immobilized onto SnO_2−C hybrid materials.[53] Of relevance to our study, it was found that the choice of substrate made an immense difference, because the resulting Pt_3Ni/SnO_2−C catalysts yielded activity values that were 2.4 times higher than those of comparable Pt_3Ni/C systems. In addition, the stability of the

DOI: 10.1021/acsami.6b07870
ACS Appl. Mater. Interfaces 2016, 8, 34280−34294

Pt_3Ni/SnO_2−C catalyst was also measurably enhanced, an observation likely due to the presence of strong, favorably synergistic interactions between Pt and the underlying SnO_2. Therefore, nuances in the chemistry and in the preparative method of the underlying surface-modified MWNT substrates herein should contribute to corresponding variations in the measured ORR activities of the analyzed, overlaid Pt NWs. Hence, it is reasonable that we predict that the −COOH−MWNT, −SH-MWNT, and $-NH_2$−MWNT samples, prepared by physical noncovalent "sonication-based" methods, should also give rise to a comparatively higher activity as compared with their counterparts synthesized using covalent "reflux-mediated" protocols.

3.2. Electrochemistry. The cyclic voltammetry scans (CVs) of all of the covalently generated samples are depicted in Figure 5A. Since our focus is on evaluating the effect of

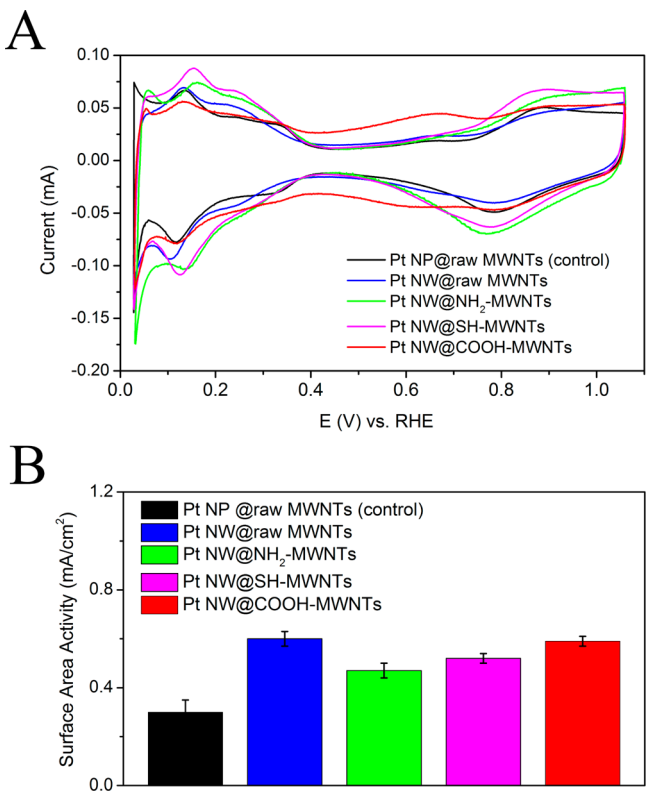

Figure 5. (A) Cyclic voltammograms of Pt nanowires supported onto various different types of functionalized MWNTs, prepared by the "**covalent reflux-mediated**" method and collected in Ar-saturated 0.1 M $HClO_4$ solution; (B) Bar graph highlighting the surface area activity of Pt nanostructures variously attached onto differentially functionalized carbon nanotubes. ORR activities have been normalized to their respective electrochemically active surface area values. Data are shown with accompanying error bars.

varying different terminal moieties upon the resulting ORR performance, we will be comparing and analyzing regions where the surfaces of our catalyst interact with oxygen-containing species (i.e., water), which is within the potential window of 0.5 to 1.0 V (vs RHE) in this case. We noticed that all the CVs possess approximately the same shape, except for the Pt NW@COOH-MWNT samples, the latter of which likely possess a higher absolute capacitance as a result of their lower overall Pt loading.

Indeed, the CVs of samples possessing carboxylic acid functional groups give rise to a peak at around 0.6−0.7 V (vs RHE) in both cathodic and anodic sweeps, which should correspond to surface oxidation formation and oxide reduction processes, respectively. However, from prior work, neither ultrathin Pt nanowires nor nanoparticles themselves should yield such a result.[42,54] Hence, it is plausible to assume that within COOH-containing systems, such features can be assigned to a reversible process involving the reduction of carboxylic acid to formaldehyde during the cathodic sweep and the corresponding oxidation of formaldehyde to carboxylic acid species during the anodic sweep.[55,56] The same behavior has also been observed with the analogous sample prepared using the noncovalent method (Figure 6A). Regarding overall shapes

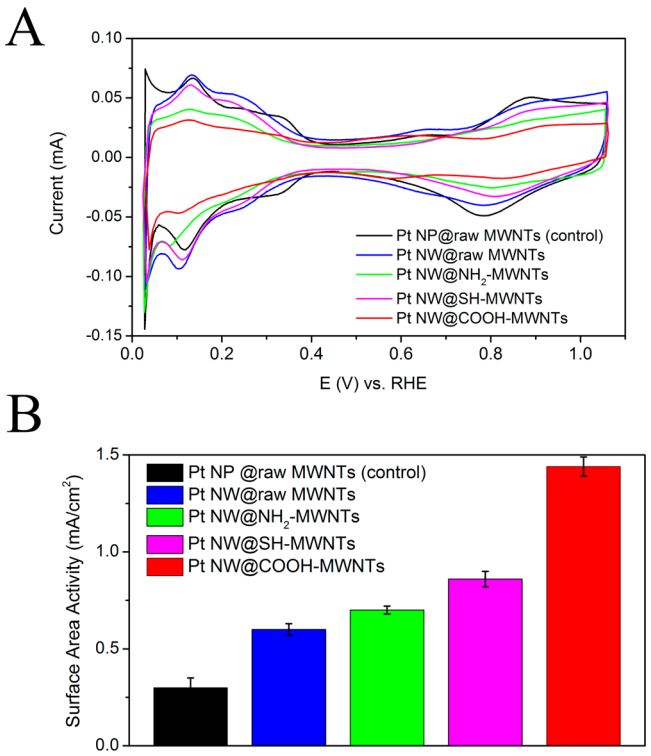

Figure 6. (A) Cyclic voltammograms of Pt nanowires supported onto various different types of functionalized MWNTs prepared by the "**noncovalent, physical sonication-induced**" method, collected in Ar-saturated 0.1 M $HClO_4$ solution; (B) Bar graph highlighting surface area activity of Pt nanostructures variously attached onto differentially functionalized carbon nanotubes. ORR activities have been normalized to their respective electrochemically active surface area values. Data are shown with accompanying error bars.

and features, we see no apparent differences between samples containing identical functional groups prepared using either covalent or noncovalent approaches. All of these data collectively indicate that the intrinsic surface profiles of the Pt NWs are actually rather similar, regardless of the preparative methods used.

As collected from their respective CVs and associated TGA results, the relevant electrochemical surface area (ECSA) data for each of our samples have been calculated and are summarized in Table 2. On the basis of our calculations, all of the nanowire-based samples basically possess more or less the same ECSA, as they are composed of essentially the same Pt NWs in every case. In effect, the only difference is that the

DOI: 10.1021/acsami.6b07870
ACS Appl. Mater. Interfaces 2016, 8, 34280−34294

Table 2. Electrochemical Surface Area (ECSA) Values, as well as Oxide Reduction Peak Positions for Pt NWs, Supported onto Variously Chemically Functionalized MWNTs, Prepared by Both Covalent and Non-covalent-Based Methods, Respectively

samples		electrochemical surface area (ECSA, m^2/g)	oxide reduction peak position (mV)
Pt NP @ raw MWNTs		55.8	784.8
Pt NW @ raw MWNTs		45.6	785.0
covalent, reflux-mediated method	Pt NW@NH_2−MWNTs	43.1	769.6
	Pt NW@SH−MWNTs	46.8	775.2
	Pt NW@COOH−MWNTs	45.7	785.5
noncovalent, sonication-induced method	Pt NW@NH_2−MWNTs	45.4	804.9
	Pt NW@SH−MWNTs	44.9	807.9
	Pt NW@COOH−MWNTs	47.1	822.3

underlying supports have altered. What is significantly and obviously different are the ECSA results for the NWs versus those for the corresponding NPs, a finding which is not surprising, considering that NWs and NPs are in fact 2 very different morphologies. Moreover, apart from the slight difference in terms of detailed features associated with CVs, we have also noticed a trend regarding the positions of the oxide reduction peaks themselves (cathodic sweep, ∼0.8 V vs RHE), which are summarized in Table 2. Specifically, we have observed a slight down-shift in the positions of the peaks of both Pt NW@SH-MWNT and Pt NW@NH_2-MWNT samples, as well as a corresponding upshift in the peak associated with the Pt NW@COOH-MWNT sample. In the past, our group and others have shown that the position of the oxide reduction peak reflects the strength of interaction between the surfaces of catalyst and that of oxygen-containing species (e.g., O_2, OH^-, and H_2O), thereby rendering it as a reasonable indicator of associated ORR performance.[43] In other words, with Pt-based systems, an upshift usually is indicative of a weaker interaction between Pt and reactive oxygen-containing species, thereby resulting in improved electrocatalytic performance and vice versa, assuming that all samples maintain similar size and morphology.

As a complementary study, linear sweep voltammetry data in the form of CO stripping spectra were also collected and have been plotted (Figure S4). The CO stripping peak potentials directly reflect and measure the degree of affinity between surface Pt atoms and CO adsorbate molecules.[57,58] As indicated by our results, the CO stripping trend correlates well with the related trend of oxide reduction potentials. That is, the higher the oxide reduction potential value (i.e., indicative of weaker Pt−O interactions), the lower the CO stripping peak position (i.e., suggestive of weaker Pt−CO interactions), and vice versa. These observations are in agreement with what we have previously found in our analogous study on Pd NWs, possessing various diameters.[59]

To examine the ORR performances of our two series of catalysts, the polarization curves associated with Pt nanowires deposited onto functionalized prepared using the covalent as well as the noncovalent methods were collected and are shown in Figures S5 and S6, respectively. However, we should note that since the Pt loading quantitatively varied for each of the variously functionalized MWNTs within the series, a direct, visual comparison from the polarization curves alone was not conclusive. Instead, we have calculated the reaction kinetic current (i_k), from the equation[60]

$$i_k = \frac{i \times i_{lim}}{i_{lim} - i} \quad (1)$$

where i is the measured current at a specified potential (0.9 V vs RHE herein) and i_{lim} is the measured limiting current (obtained at 0.4 V vs RHE). As a result, values for the (a) specific surface area activity (SA) and (b) Pt mass activity (MA) could be calculated by dividing i_k either by (a) the surface area (obtained through an integration of the hydrogen absorption area, conventionally designated as H_{ads} within CV curves) or by (b) the actual amount of Pt used (based upon the TGA results), respectively.

The resulting SA data, which underscore the intrinsic kinetic behavior of the catalysts, for all of the relevant samples created by the covalent (Figure 5B) and the noncovalent (Figure 6B) methods respectively, are presented as bar graphs. Specifically, for covalently functionalized samples, based upon their respective current density values measured at 0.9 V vs RHE, the order of magnitudes of the observed specific activities can be summarized as raw ≈ COOH > SH > NH_2. By contrast, for the noncovalent method, the corresponding trend is COOH > SH > NH_2 > raw, which precisely correlates with the expected trend for their corresponding oxidation/reduction peak positions.

Overall, the highest activity we achieved herein can be expressed as 1.54 mA/cm^2 in terms of specific activity (SA) and 0.66 A/mg_{Pt} in terms of the Pt mass activity (MA). These data are associated with the Pt NW@COOH−MWNTs synthesized with the noncovalent method, representing not only a nearly 2.5-fold increase as compared with Pt NW@raw-MWNTs (i.e., 0.60 mA/cm^2 for SA and 0.27 A/mg_{Pt} for MA) but also, more significantly, a 5-fold increase as compared with conventional 0D@1D nanostructures, such as, for example, Pt NP@raw-MWNTs (i.e., 0.30 mA/cm^2 for SA and 0.17 A/mg_{Pt} for MA). A summary of all of our SA and MA results collected herein for our variously functionalized samples is presented in Figure 7, with a clear comparison provided with analogous commercial standards. Moreover, to the best of our knowledge, as highlighted in Table 3, the very high ORR activity value specifically observed for ultrathin Pt nanowires deposited onto COOH−MWNTs through a noncovalent process surpasses the corresponding performance of not only the state-of-the-art commercial Pt/C (acquired from the Johnson Matthey (JM) company)[61] but also all other comparable systems previously reported in the literature, specifically incorporating both nanoscale Pt metal catalysts AND carbon-based supports.

In an additional experiment, the stability of our best-performing Pt NW@COOH-MWNT sample was investigated by means of an accelerated degradation test (ADT), using linear potential sweeps during potential cycling between 0.6 and 1.0 V (vs RHE) at 50 mV s^{-1} in an aqueous O_2-saturated 0.1 M $HClO_4$ solution (Figure 8). We found that the Pt NW@COOH-MWNTs were able to maintain 83% and 78% of their

DOI: 10.1021/acsami.6b07870
ACS Appl. Mater. Interfaces 2016, 8, 34280−34294

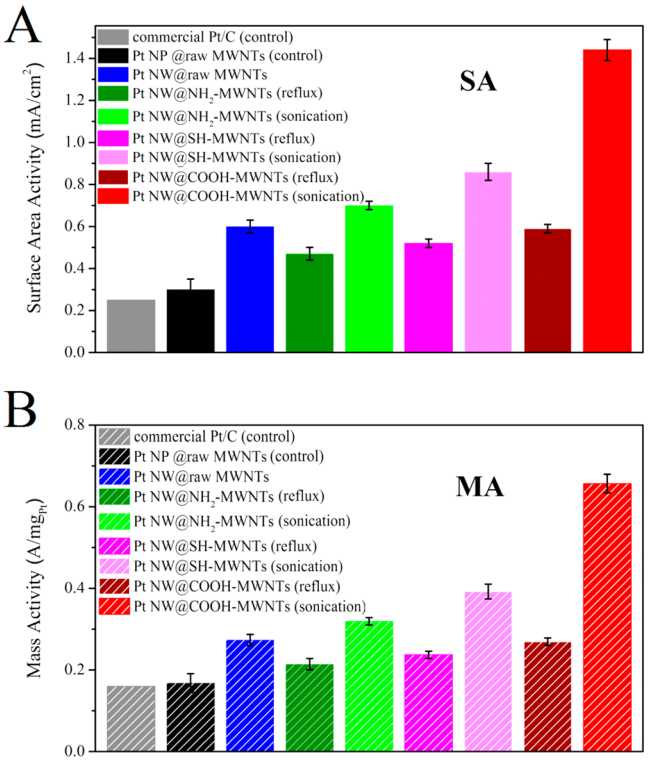

Figure 7. Vertical bars highlighting (A) surface area activity and (B) mass activity of Pt nanostructures variously attached onto differentially functionalized carbon nanotubes.

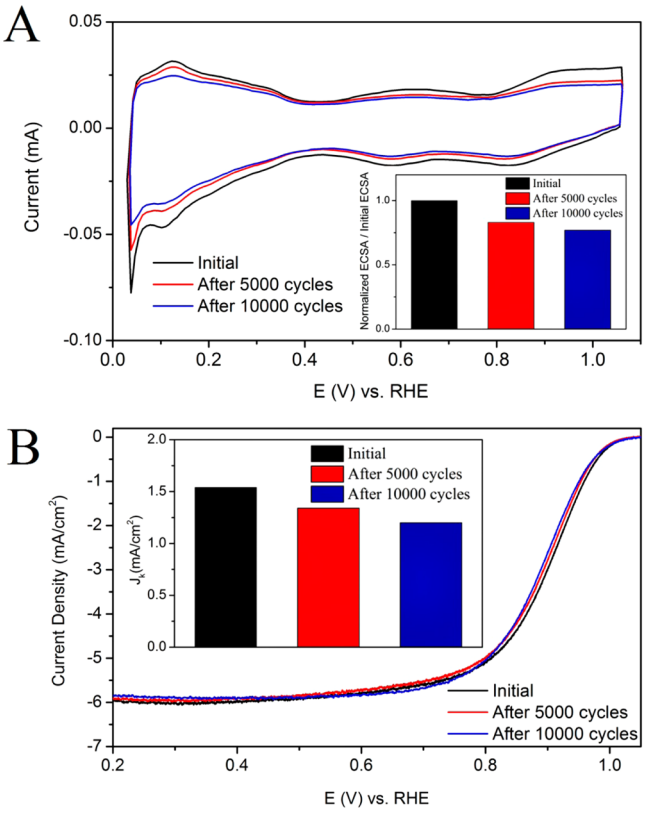

Figure 8. (A) Cyclic voltammograms obtained in a deoxygenated 0.1 M $HClO_4$ solution after successive 5000 cycle runs for the high-performing Pt NW@COOH-MWNT nanocomposite. In the inset, the measured ECSA loss is shown as a function of durability cycling for the electrocatalyst. (B) The corresponding polarization curves, obtained in an oxygen-saturated 0.1 M $HClO_4$ solution at 1600 rpm after successive 5000 cycle runs. Surface area specific activities, measured at 0.9 V, are plotted as a function of durability in the figure inset.

initial measured ECSA values after 5000 and 10000 cycles, respectively (Figure 8A). In terms of activities, only a 12 mV degradation in the half-wave potential as well as a 23% decrease in terms of ORR specific activities (Figure 8B) have been measured for this composite. By contrast, the analogous commercial Pt/C catalyst has been reported to exhibit an ~36 mV degradation in the observed half-wave potential and a 50% decrease in activity.[61] Our results therefore indicate that our most optimized catalyst configuration not only possesses favorably improved ORR performance but also retains outstanding long-term stability as compared with a commercial standard control.

3.3. Mechanistic Discussion of Proposed Charge Transfer. *3.3.1. Samples Prepared by Covalent Attachment.* For the samples produced using the covalent "reflux method", because of the numbers of degrees of freedom associated with bond motion, it is unlikely that the aromatic ring inherent to the structure of the terminal moiety is completely geometrically aligned with the underlying π-conjugated MWNT system. Therefore, we do not expect π-electrons between these two structures to directly, fully, and effectively interact with each other (Scheme 1). Instead, we believe that the key driving force herein is the presence of amide bonds (−CO−NH−) that connect the linker with the MWNTs. Whereas the −C═O− group can be considered as an electron withdrawing unit,[62] it has nonetheless been shown by previous reports that the lone pair on the nitrogen atom within the amide group (−NH−CO−) can also potentially serve as an electron donating species to the conjugated π-electron system (i.e., the benzene ring) connected to it.[49] The combination of both chemical and

Table 3. Summary of Mass Activity and Surface Specific Activity Values for the ORR Reaction, Associated with Representative Systems (i.e., Pt Metal Catalysts Immobilized onto Carbon-Based Supports)

catalysts	substrate	mass activity (in A current per mg of Pt)	surface specific activity (in mA current per cm_{Pt}^2)	ref
commercial Pt nanoparticles (Johnson Matthey)	carbon black	~0.16	~0.25	61
Pt nanoparticles	graphene	~0.20	~0.50	69
Pt nanoparticles	Ketjenblack	~0.28	~0.58	
Pt nanoparticles	raw MWNTs	~0.14	~0.50	
Pt nanoparticles	3D ordered mesoporous carbon sphere array (OMCS)	~0.21	~0.25	70
ultrathin Pt nanowires	COOH-derivatized MWNTs (physical sonication method)	~0.68	~1.54	this work

DOI: 10.1021/acsami.6b07870
ACS Appl. Mater. Interfaces 2016, 8, 34280−34294

structural effects results in electron movement from MWNTs not only to the conjugated aromatic benzene ring associated with the terminal functional group but also presumably to some degree onto the attached, immobilized Pt atoms. In so doing, these processes can have a noticeable impact upon and thereby effectively "tune" the electronic structure of Pt.

As discussed earlier, the Pt NW@MWNT−COOH sample gives rise to the smallest shift in terms of the XPS peak position (i.e., Pt $4f_{7/2}$ = 71.3 eV), whereas perceptibly larger shifts were noted with both Pt@MWNT−SH (i.e., Pt $4f_{7/2}$ = 69.7 eV) and Pt@MWNT−NH_2 (i.e., Pt $4f_{7/2}$ = 69.5 eV), respectively, using the peak position of raw MWNT samples as a control (i.e., Pt $4f_{7/2}$ = 71.2 eV). The magnitude of the shift denotes the extent of electron transfer at the interface between the Pt and the underlying MWNTs. Both experimental[63] and theoretical[64] studies have separately demonstrated that when bonded with Pt, atoms such as O, N, and S tend to undergo a metal-to-ligand charge transfer process (MLCT), which counteracts the structurally induced charge transfer process from the functionalized MWNT surface to the immobilized Pt.

It should be noted that DFT calculations describing both NH_2 and SH species adsorbed onto Pt (111) surfaces have suggested a bond strength value of 2.00 eV for −NH_2 species and of 2.31 eV for −SH species under similar modeling conditions, respectively. These computations would indicate that the interaction between Pt and S is likely to be stronger than that between Pt and N.[65,66] Furthermore, the overall bond strength of formate (COO^-) species adsorbed onto Pt is likely ∼2.54 eV, as individual constituent Pt−O bonds possess discrete bond strengths of 1.27 eV.[67] As we have only utilized an acidic solution (0.1 M $HClO_4$) as our electrochemical environment in which to run our reactions, it is reasonable to assume that with carboxyl groups, the actual species connected to Pt atoms consists of $-COO^-$ as opposed to −COOH. Hence, the presence of formate ions likely gives rise to an even stronger interaction with Pt as compared with either −SH or −NH_2.

Therefore, we presume that the effect of varying the identity of the terminal linker moiety from the perspective of the intensity of the bonding with the underlying Pt support would be in order of decreasing importance: Pt NW@COOH−MWNT > Pt NW@SH−MWNT > Pt NW@NH_2−MWNT. It is a trend, which not only precisely mirrors the corresponding XPS shifts measured but also is consistent with the ORR activities observed.

3.3.2. Samples Prepared by Noncovalent Attachment. As for samples prepared using the noncovalent method, we anticipate that the benzene rings in the terminal functionalities and the MWNTs would overlap with each other, thereby promoting favorable $\pi-\pi$ stacking interactions between the electron clouds of both structures. Hence, by contrast with the electron-withdrawing effect associated with the intervening carbonyls noted with the covalent method, electron transfer would be expected to occur from the conjugated benzene rings within the terminal functionalities to the attached MWNTs, a finding consistent with a previous report.[68]

In addition, as we have previously discussed, we expect to observe metal-to-ligand charge transfer (MLCT) between Pt and associated terminal moieties. Hence, the charge transfer direction of the −COOH, −SH, and −NH_2 species in this case would be expected to be in the direction from Pt to the underlying functionalized supports, as a result of these two synergistic and cooperative effects, incorporating both the $\pi-\pi$ stacking interactions and the MLCT process. Moreover, as discussed previously, the extent of such a charge transfer process would follow the trend of COOH > SH > NH_2, thereby rendering the Pt NW@COOH−MWNT species as the most favorable toward ORR, which again is in good agreement with our electrochemical data.

Furthermore, when comparing all samples generated by both covalent and noncovalent methods, we observed an enhancement of ORR activity with the sample prepared by the noncovalent method as compared with that generated by the analogous covalent protocol. Notwithstanding the importance of the alteration of the electronic structure of Pt in the presence of the functionalized MWNTs, we can also attribute our observations to the nature of the MWNTs themselves. In other words, the covalent "reflux method" tends to damage the external structure and compromises the structural integrity of the MWNTs to some extent, whereas the noncovalent, "sonication-mediated" protocol is associated with less destructive $\pi-\pi$ stacking interactions. Overall, based upon data from all three types of terminal moieties tested (i.e., −SH, −NH_2, and −COOH), we assert that the noncovalent, physical "sonication-based" methodology represents a superior attachment approach as compared with one based on covalent chemistry.

4. CONCLUSIONS

The goal of our study has been to probe catalyst−support interactions mediated by terminal functionalities on derivatized MWNT support surfaces. To this end, we have utilized two different attachment approaches, namely "covalent reflux-mediated" and "noncovalent sonication-induced" methods, to prepare a series of carboxylic acid-, amine-, and thiol-terminated MWNTs. The nature of the binding interactions as well as the possibility of charge transfer within as-functionalized MWNTs were analyzed by means of XPS spectroscopy. Our results demonstrated that the precise attachment method used often yielded completely different electronic signatures and behaviors, owing to the distinctive and very particular interactions between MWNTs and their associated terminal functionalities.

Specifically, for chemically synthesized, covalent-based systems, electron transfer likely occurs from the MWNTs to the attached terminal end groups due to the presence of the electron-withdrawing amides. On the other hand, for sonication-induced, noncovalently derived samples, charge transfer likely takes place from the attached moieties to the MWNTs, owing to preferable electron donation from the conjugated benzene rings of the terminal derivatizing moiety to the attached MWNTs, which likely emanate from favorable $\pi-\pi$ stacking interactions.

Moreover, the surface-modified MWNTs have been utilized as the underlying support motif for ultrathin Pt nanowires, and the catalytic performance toward ORR of these very small diameter, anisotropic electrocatalysts has been electrochemically probed. As a result of possible charge transfer, the ORR performance metrics were noted to be a function of the end group termination of the MWNT support. Indeed, the activity trend of the Pt nanowire-based series is, as follows, for the covalent "reflux" method: raw ≈ COOH > SH > NH_2. For the analogous sonication-induced, noncovalent method, the trend is COOH > SH > NH_2 > raw, which precisely correlates with the expected trend for their corresponding oxidation and reduction peak positions.

DOI: 10.1021/acsami.6b07870
ACS Appl. Mater. Interfaces 2016, 8, 34280−34294

Overall, based upon data collected on all three types of terminal moieties tested (i.e., −SH, $-NH_2$, and −COOH), we believe that the noncovalent physical "sonication-based" method represents a clearly superior attachment approach as compared with one based on covalent chemistry. In particular, samples prepared using the noncovalent method give rise to a more beneficial electronic modification of the immobilized Pt, as evinced by XPS results, which substantiate the corresponding trends in electrochemical performance.

Indeed, the highest activity we measured herein is 1.54 mA/cm^2, which can be attributed to the Pt NW@COOH-MWNT sample synthesized using the noncovalent method. This value denotes a nearly 2.5-fold improvement as compared with Pt NW@raw-MWNTs (i.e., 0.60 mA/cm^2), as well as to a 5-fold increase as compared with 0D@1D nanostructures, such as, for example, Pt NP@raw-MWNTs (i.e., 0.30 mA/cm^2). Moreover, this activity outcome also denotes a ∼1.8-fold increase in performance enhancement as compared with the corresponding data (i.e., 0.87 mA/cm^2 from Figure S7) for a control sample (n.b. sample preparation described in the Supporting Information), consisting of ultrathin Pt nanowires deposited onto carboxylic acid-functionalized carbon black (i.e., the Pt NW@COOH-CB composite). Moreover, to the best of our knowledge, this promising result with our Pt NW@COOH-MWNT sample represents the *highest surface specific activity value measured, to date, using any carbon-based support*. Furthermore, in terms of the cost-effectiveness of our system, our Pt NW@COOH-MWNT sample yielded a Pt mass activity value of 0.68 A/mg_{Pt}, signifying a more than 4-fold increase over comparable data (i.e., 0.16 A/mg_{Pt}), measured for state-of-the-art commercial Pt/C systems.

Finally, as an added element of novelty, we have reported for the first time on the combination of ultrathin Pt NWs with functionalized carbon nanotubes and found that these composites gave rise to largely enhanced activity, especially when compared with analogous samples of conventional Pt nanoparticles immobilized onto MWNTs. Hence, we have demonstrated that tuning catalyst−support interactions through rational functionalization of CNTs represents a fundamentally sound strategy for designing better ORR catalysts.

■ ASSOCIATED CONTENT

Supporting Information

The Supporting Information is available free of charge on the ACS Publications website at DOI: 10.1021/acsami.6b07870.

Functionalization protocol and electrochemical profiles for a carboxylic acid-terminated "carbon black" control sample, TGA curves, representative TEM images, and relevant electrochemical polarization curves for all of the samples analyzed, including control samples (PDF)

■ AUTHOR INFORMATION

Corresponding Author

*E-mail: stanislaus.wong@stonybrook.edu; sswong@bnl.gov.

ORCID

Stanislaus S. Wong: 0000-0001-7351-0739

Notes

The authors declare no competing financial interest.

■ ACKNOWLEDGMENTS

Research funding for all authors was provided by the U.S. Department of Energy, Basic Energy Sciences, Materials Sciences and Engineering Division. We thank Gerard Mattei for electrochemical data acquisition associated with the "Pt NW@COOH−CB composite" control sample. Work was conducted at Brookhaven National Laboratory, funded under Contract No. DE-SC-00112704. XPS data were collected at BNL's Center for Functional Nanomaterials, supported under Contract No. DE-SC-00112704. Raman data were acquired at Stony Brook University's Nano-Raman Molecular Imaging Laboratory (NARMIL), established with NSF MRI Grant OCE-1336724.

■ REFERENCES

(1) Ehteshami, S. M. M.; Jia, Q. Y.; Halder, A.; Chan, S. H.; Mukerjee, S. The role of electronic properties of Pt and Pt alloys for enhanced reformate electro-oxidation in polymer electrolyte membrane fuel cells. *Electrochim. Acta* **2013**, *107*, 155−163.

(2) Rao, Z. H.; Wang, S. F. A review of power battery thermal energy management. *Renewable Sustainable Energy Rev.* **2011**, *15*, 4554−4571.

(3) Darrow, K.; Tidball, R.; Wang, J.; Hampson, A. *Catalog of CHP Technologies: Combined Heat and Power Partnership*; U.S. Environmental Protection Agency: September, 2014; Section 6.

(4) Song, C. Fuel processing for low-temperature and high-temperature fuel cells: Challenges, and opportunities for sustainable development in the 21st century. *Catal. Today* **2002**, *77*, 17−49.

(5) Norskov, J. K.; Rossmeisl, J.; Logadottir, A.; Lindqvist, L.; Kitchin, J. R.; Bligaard, T.; Jonsson, H. Origin of the Overpotential for Oxygen Reduction at a Fuel-Cell Cathode. *J. Phys. Chem. B* **2004**, *108*, 17886−17892.

(6) He, C.; Desai, S.; Brown, G.; Bollepalli, S. PEM Fuel Cell Catalysts: Cost, Performance, and Durability. *Electrochem. Soc. Interface* **2005**, *14*, 41−44.

(7) Weber, J.; Singhal, R.; Zekri, S.; Kumar, A. One-Dimensional Nanostructures: Fabrication, Characterization and Applications. *Int. Mater. Rev.* **2008**, *53*, 235−255.

(8) Cademartiri, L.; Ozin, G. A. Ultrathin Nanowires - A Materials Chemistry Perspective. *Adv. Mater.* **2009**, *21* (9), 1013−1020.

(9) Xia, Y.; Yang, P.; Sun, Y.; Wu, Y.; Mayers, B.; Gates, G.; Yin, Y.; Kim, F.; Yan, H. One-Dimensional Nanostructures: Synthesis, Characterization, and Applications. *Adv. Mater.* **2003**, *15* (5), 353−389.

(10) Lim, B.; Jiang, M.; Camargo, P. H. C.; Cho, E. C.; Tao, J.; Lu, X.; Zhu, Y.; Xia, Y. Pd-Pt Bimetallic Nanodendrites with High Activity for Oxygen Reduction. *Science* **2009**, *324* (5932), 1302−1305.

(11) Koenigsmann, C.; Scofield, M. E.; Liu, H. Q.; Wong, S. S. Designing Enhanced One-Dimensional Electrocatalysts for the Oxygen Reduction Reaction: Probing Size- and Composition-Dependent Electrocatalytic Behavior in Noble Metal Nanowires. *J. Phys. Chem. Lett.* **2012**, *3* (22), 3385−3398.

(12) Sharma, S.; Pollet, B. G. Support materials for PEMFC and DMFC electrocatalysts-A review. *J. Power Sources* **2012**, *208*, 96−119.

(13) Shah, P. H.; Batra, R. C. Effect of Covalent Functionalization on Young's Modulus of a Single-Wall Carbon Nanotube. *Springer Ser. Mater. Sci.* **2014**, *188*, 111−134.

(14) Shen, W.; Li, X.; Liu, X. A study of oxidizing centers in carbon nanotubes by solid-state NMR. *RSC Adv.* **2015**, *5* (74), 60380−60385.

(15) Jarosz, P.; Schauerman, C.; Alvarenga, J.; Moses, B.; Mastrangelo, T.; Raffaelle, R.; Ridgley, R.; Landi, B. Carbon nanotube wires and cables: near-term applications and future perspectives. *Nanoscale* **2011**, *3* (11), 4542−4553.

(16) Reilly, R. M. Carbon nanotubes: potential benefits and risks of nanotechnology in nuclear medicine. *J. Nucl. Med.* **2007**, *48* (7), 1039−1042.

DOI: 10.1021/acsami.6b07870
ACS Appl. Mater. Interfaces 2016, 8, 34280−34294

(17) Nie, Y.; Li, L.; Wei, Z. Recent advancements in Pt and Pt-free catalysts for oxygen reduction reaction. *Chem. Soc. Rev.* **2015**, *44* (8), 2168−2201.
(18) Li, L.; Chen, C.; Wei, Z. D.; Qi, X. Q.; Xia, M. R.; Wang, Y. Q. Experimental and DFT study of thiol-stabilized Pt/CNTs catalysts. *Phys. Chem. Chem. Phys.* **2012**, *14*, 16581−16587.
(19) Manesh, K. M.; Santhosh, P.; Gopalan, A. I.; Lee, K.-P. Electrocatalytic Dioxygen Reduction at Glassy Carbon Electrode Modified with Polyaniline Grafted Multiwall Carbon Nanotube Film. *Electroanalysis* **2006**, *18* (16), 1564−1571.
(20) Choudhury, A.; Kar, P. Doping effect of carboxylic acid group functionalized multi-walled carbon nanotube on polyaniline. *Composites, Part B* **2011**, *42* (6), 1641−1647.
(21) Mu, Y.; Liang, H.; Hu, J.; Jiang, L.; Wan, L. Controllable Pt Nanoparticle Deposition on Carbon Nanotubes as an Anode Catalyst for Direct Methanol Fuel Cells. *J. Phys. Chem. B* **2005**, *109* (47), 22212−22216.
(22) Georgakilas, V.; Gournis, D.; Tzitzios, V.; Pasquato, L.; Guldi, D. M.; Prato, M. Decorating carbon nanotubes with metal or semiconductor nanoparticles. *J. Mater. Chem.* **2007**, *17* (26), 2679−2694.
(23) Wu, B.; Hu, D.; Kuang, Y.; Liu, B.; Zhang, X.; Chen, J. Functionalization of Carbon Nanotubes by an Ionic-Liquid Polymer: Dispersion of Pt and PtRu Nanoparticles on Carbon Nanotubes and Their Electrocatalytic Oxidation of Methanol. *Angew. Chem., Int. Ed.* **2009**, *48* (26), 4751−4754.
(24) Ding, K. Q.; Yang, H. W.; Cao, Y. L.; Zheng, C. B.; Liu, L.; Liu, L. K.; Wang, Y. R.; Yan, X. R.; Guo, Z. H. Multi-Walled Carbon Nanotube-Gold Nanocomposites toward Oxygen Reduction Reaction. *Int. J. Electrochem. Soc.* **2013**, *8* (4), 5343−5358.
(25) Alexeyeva, N.; Matisen, L.; Saar, A.; Laaksonen, P.; Kontturi, K.; Tammeveski, K. Kinetics of oxygen reduction on gold nanoparticle/multi-walled carbon nanotube hybrid electrodes in acid media. *J. Electroanal. Chem.* **2010**, *642* (1), 6−12.
(26) Alexeyeva, N.; Laaksonen, T.; Kontturi, K.; Mirkhalaf, F.; Schiffrin, D. J.; Tammeveski, K. Oxygen reduction on gold nanoparticle/multi-walled carbon nanotubes modified glassy carbon electrodes in acid solution. *Electrochem. Commun.* **2006**, *8* (9), 1475−1480.
(27) Karousis, N.; Tsotsou, G. E.; Evangelista, F.; Rudolf, P.; Ragoussis, N.; Tagmatarchis, N. Carbon nanotubes decorated with palladium nanoparticles: Synthesis, characterization, and catalytic activity. *J. Phys. Chem. C* **2008**, *112* (35), 13463−13469.
(28) Orellana, W. Metal-phthalocyanine functionalized carbon nanotubes as catalyst for the oxygen reduction reaction: A theoretical study. *Chem. Phys. Lett.* **2012**, *541*, 81−84.
(29) Guo, L.; Chen, S. G.; Li, L.; Wei, Z. D. A CO-tolerant PtRu catalyst supported on thiol-functionalized carbon nanotubes for the methanol oxidation reaction. *J. Power Sources* **2014**, *247*, 360−364.
(30) Kim, J.; Lee, S. W.; Carlton, C.; Shao-Horn, Y. Pt-Covered Multiwall Carbon Nanotubes for Oxygen Reduction in Fuel Cell Applications. *J. Phys. Chem. Lett.* **2011**, *2* (11), 1332−1336.
(31) Li, L.; Chen, S. G.; Wei, Z. D.; Qi, X. Q.; Xia, M. R.; Wang, Y. Q. Experimental and DFT study of thiol-stabilized Pt/CNTs catalysts. *Phys. Chem. Chem. Phys.* **2012**, *14* (48), 16581−16587.
(32) Zhang, S. Y.; Hou, L. L.; Hou, M. H.; Liang, H. J. Hydrothermal synthesis of spindle-like Zn_2SiO_4 nanoparticles and its application in lithium-ion battery. *Mater. Lett.* **2015**, *156*, 82−85.
(33) Sharma, S.; Pollet, B. G. Support materials for PEMFC and DMFC electrocatalysts—A review. *J. Power Sources* **2012**, *208*, 96−119.
(34) Sheng, W. C.; Lee, S. W.; Crumlin, E. J.; Chen, S.; Shao-Horn, Y. Synthesis, Activity and Durability of Pt Nanoparticles Supported on Multi-walled Carbon Nanotubes for Oxygen Reduction. *J. Electrochem. Soc.* **2011**, *158* (11), B1398−B1404.
(35) Kim, J.; Lee, S. W.; Carlton, C.; Shao-Horn, Y. Oxygen Reduction Activity of Pt_xNi_{1-x} Alloy Nanoparticles on Multiwall Carbon Nanotubes. *Electrochem. Solid-State Lett.* **2011**, *14* (10), B110−B113.
(36) Deborah, M.; Jawahar, A.; Mathavan, T.; Dhas, M. K.; Benial, A. M. Spectroscopic studies on sidewall carboxylic acid functionalization of multi-walled carbon nanotubes with valine. *Spectrochim. Acta, Part A* **2015**, *139*, 138−144.
(37) Park, S.-A.; Kim, D.-S.; Kim, T.-J.; Kim, Y.-T. Strong Interaction between Pt and Thiolated Carbon for Electrocatalytic Durability Enhancement. *ACS Catal.* **2013**, *3* (12), 3067−3074.
(38) Kim, Y.; Mitani, T. Surface thiolation of carbon nanotubes as supports: A promising route for the high dispersion of Pt nanoparticles for electrocatalysts. *J. Catal.* **2006**, *238* (2), 394−401.
(39) Teng, X.; Han, W. Q.; Ku, W.; Hucker, M. Synthesis of ultrathin palladium and platinum nanowires and a study of their magnetic properties. *Angew. Chem., Int. Ed.* **2008**, *47* (11), 2055−2058.
(40) Chen, S.; Wei, Z.; Guo, L.; Ding, W.; Dong, L.; Shen, P.; Qi, X.; Li, L. Enhanced dispersion and durability of Pt nanoparticles on a thiolated CNT support. *Chem. Commun.* **2011**, *47* (39), 10984−10986.
(41) Koenigsmann, C.; Santulli, A. C.; Gong, K. P.; Vukmirovic, M. B.; Zhou, W. P.; Sutter, E.; Wong, S. S.; Adzic, R. R. Enhanced Electrocatalytic Performance of Processed, Ultrathin, Supported Pd-Pt Core-Shell Nanowire Catalysts for the Oxygen Reduction Reaction. *J. Am. Chem. Soc.* **2011**, *133* (25), 9783−9795.
(42) Koenigsmann, C.; Zhou, W. P.; Adzic, R. R.; Sutter, E.; Wong, S. S. Size-Dependent Enhancement of Electrocatalytic Performance in Relatively Defect-Free, Processed Ultrathin Platinum Nanowires. *Nano Lett.* **2010**, *10*, 2806−2811.
(43) Liu, H. Q.; Koenigsmann, C.; Adzic, R. R.; Wong, S. S. Probing Ultrathin One-Dimensional Pd-Ni Nanostructures As Oxygen Reduction Reaction Catalysts. *ACS Catal.* **2014**, *4*, 2544−2555.
(44) Punnoose, A.; Seehra, M. S.; Wender, I. Structure, properties and roles of the different constituents in $Pt/WO_x/ZrO_2$ catalysts. *Fuel Process. Technol.* **2001**, *74* (1), 33−47.
(45) Carper, J. The CRC Handbook of Chemistry and Physics. *Libr J.* **1999**, *124* (10), 192.
(46) Higuchi, E.; Uchida, H.; Watanabe, M. Effect of loading level in platinum-dispersed carbon black electrocatalysts on oxygen reduction activity evaluated by rotating disk electrode. *J. Electroanal. Chem.* **2005**, *583* (1), 69−76.
(47) Soin, N.; Roy, S. S.; Ray, S. C.; McLaughlin, J. A. Excitation energy dependence of Raman bands in multiwalled carbon nanotubes. *J. Raman Spectrosc.* **2010**, *41* (10), 1227−1233.
(48) Datsyuk, V.; Kalyva, M.; Papagelis, K.; Parthenios, J.; Tasis, D.; Siokou, A.; Kallitsis, I.; Galiotis, C. Chemical oxidation of multiwalled carbon nanotubes. *Carbon* **2008**, *46* (6), 833−840.
(49) do Nascimento, G. M.; Hou, T.; Kim, Y. A.; Muramatsu, H.; Hayashi, T.; Endo, M.; Akuzawa, N.; Dresselhaus, M. S. Behavior of the high frequency Raman modes of double-wall carbon nanotubes after doping with bromine or iodine vapors. *Carbon* **2011**, *49* (11), 3585−3596.
(50) Silva, W. M.; Ribeiro, H.; Seara, L. M.; Calado, H. D. R.; Ferlauto, A. S.; Paniago, R. M.; Leite, C. F.; Silva, G. G. Surface Properties of Oxidized and Aminated Multi-Walled Carbon Nanotubes. *J. Braz. Chem. Soc.* **2012**, *23*, 1078−1086.
(51) Thomas, H. R.; Marsden, A. J.; Walker, M.; Wilson, N. R.; Rourke, J. P. Sulfur-functionalized graphene oxide by epoxide ring-opening. *Angew. Chem., Int. Ed.* **2014**, *53* (29), 7613−7618.
(52) Awaludin, Z.; Suzuki, M.; Masud, J.; Okajima, T.; Ohsaka, T. Enhanced Electrocatalysis of Oxygen Reduction on $Pt/TaO_x/GC$. *J. Phys. Chem. C* **2011**, *115* (51), 25557−25567.
(53) Zhang, N.; Du, L.; Du, C. Y.; Yin, G. P. Tin dioxide facilitated truncated octahedral Pt_3Ni alloy catalyst: synthesis and ultra highly active and durable electrocatalysts for oxygen reduction reaction. *RSC Adv.* **2016**, *6* (31), 26323−26328.
(54) Guo, S. J.; Zhang, S.; Sun, S. H. Tuning Nanoparticle Catalysis for the Oxygen Reduction Reaction. *Angew. Chem., Int. Ed.* **2013**, *52*, 8526−8544.
(55) Zhang, W. M.; Chen, J.; Swiegers, G. F.; Ma, Z. F.; Wallace, G. G. Microwave-assisted synthesis of Pt/CNT nanocomposite electrocatalysts for PEM fuel cells. *Nanoscale* **2010**, *2*, 282−286.

DOI: 10.1021/acsami.6b07870
ACS Appl. Mater. Interfaces 2016, 8, 34280−34294

(56) Hoa, L. Q.; Vestergaard, M. C.; Yoshikawa, H.; Saito, M.; Tamiya, E. Enhancing catalytic performance of Pt-based electrodes with a noncovalent interaction-induced functionalized carbon nanotube-grafted matrix. *J. Mater. Chem.* **2012**, *22*, 14705−14714.
(57) Newton, J. E.; Preece, J. A.; Rees, N. V.; Horswell, S. L. Nanoparticle catalysts for proton exchange membrane fuel cells: can surfactant effects be beneficial for electrocatalysis? *Phys. Chem. Chem. Phys.* **2014**, *16* (23), 11435−11446.
(58) Maillard, F.; Eikerling, M.; Cherstiouk, O. V.; Schreier, S.; Savinova, E.; Stimming, U. Size effects on reactivity of Pt nanoparticles in CO monolayer oxidation: The role of surface mobility. *Faraday Discuss.* **2004**, *125*, 357−377.
(59) Koenigsmann, C.; Santulli, A. C.; Sutter, E.; Wong, S. S. Ambient Surfactantless Synthesis, Growth Mechanism, and Size-Dependent Electrocatalytic Behavior of High-Quality, Single Crystalline Palladium Nanowires. *ACS Nano* **2011**, *5* (9), 7471−7487.
(60) Khudhayer, W. J.; Kariuki, N. N.; Wang, X. P.; Myers, D. J.; Shaikh, A. U.; Karabacak, T. Oxygen Reduction Reaction Electrocatalytic Activity of Glancing Angle Deposited Platinum Nanorod Arrays. *J. Electrochem. Soc.* **2011**, *158* (8), B1029−B1041.
(61) He, D. S.; He, D. P.; Wang, J.; Lin, Y.; Yin, P. Q.; Hong, X.; Wu, Y.; Li, Y. D. Ultrathin Icosahedral Pt-Enriched Nanocage with Excellent Oxygen Reduction Reaction Activity. *J. Am. Chem. Soc.* **2016**, *138* (5), 1494−1497.
(62) Johnson, A. W. *Invitation to Organic Chemistry*; Jones and Bartlett: Sudbury, MA, 1999.
(63) Chatterjee, S.; Krause, J. A.; Oliver, A. G.; Connick, W. B. Intramolecular NH center dot center dot center dot Pt Interactions of Platinum(II) Diimine Complexes with Phenyl Ligands. *Inorg. Chem.* **2010**, *49*, 9798−9808.
(64) Yang, Z. X.; Wu, R. Q.; Rodriguez, J. A. First-principles study of the adsorption of sulfur on Pt(111): S core-level shifts and the nature of the Pt-S bond. *Phys. Rev. B: Condens. Matter Mater. Phys.* **2002**, *65*, 155409/1-9.
(65) Novell-Leruth, G.; Valcarcel, A.; Clotet, A.; Ricart, J. M.; Perez-Ramirez, J. DFT Characterization of Adsorbed NHx Species on Pt(100) and Pt(111) Surfaces. *J. Phys. Chem. B* **2005**, *109*, 18061−18069.
(66) Liu, Y.; Guo, W.; Lu, X.; Gao, W.; Li, G.; Guo, Y.; Zhu, J.; Hao, L. Density functional theory study of hydrogenation of S to H_2S on Pt-Pd alloy surfaces. *RSC Adv.* **2016**, *6*, 6289−6299.
(67) Silbaugh, T. L.; Karp, E. M.; Campbell, C. T. Energetics of Formic Acid Conversion to Adsorbed Formates on Pt(111) by Transient Calorimetry. *J. Am. Chem. Soc.* **2014**, *136* (10), 3964−3971.
(68) Tournus, F.; Latil, S.; Heggie, M. I.; Charlier, J. C. pi-stacking interaction between carbon nanotubes and organic molecules. *Phys. Rev. B: Condens. Matter Mater. Phys.* **2005**, *72*, 075431/1-5.
(69) Nagasawa, K.; Takao, S.; Higashi, K.; Nagamatsu, S.; Samjeske, G.; Imaizumi, Y.; Sekizawa, O.; Yamamoto, T.; Uruga, T.; Iwasawa, Y. Performance and durability of Pt/C cathode catalysts with different kinds of carbons for polymer electrolyte fuel cells characterized by electrochemical and in situ XAFS techniques. *Phys. Chem. Chem. Phys.* **2014**, *16* (21), 10075−10087.
(70) Zhang, C.; Xu, L.; Shan, N.; Sun, T.; Chen, J.; Yan, Y. Enhanced Electrocatalytic Activity and Durability of Pt Particles Supported on Ordered Mesoporous Carbon Spheres. *ACS Catal.* **2014**, *4*, 1926−1930.

DOI: 10.1021/acsami.6b07870
ACS Appl. Mater. Interfaces 2016, 8, 34280−34294